# An electron microscopy appraisal of tensile fracture in metallic glasses

Matthews, D. T. A.; Ocelik, V.; Bronsveld, P. M.; De Hosson, J. Th. M.

*Published in:*
Acta Materialia

*DOI:*
10.1016/j.actamat.2007.12.029



*Publication date:*
2008

Available online at www.sciencedirect.com
ScienceDirect
Acta Materialia 56 (2008) 1762–1773
Acta MATERIALIA
www.elsevier.com/locate/actamat

# An electron microscopy appraisal of tensile fracture in metallic glasses

D.T.A. Matthews, V. Ocelík, P.M. Bronsveld, J.Th.M. De Hosson *

*Department of Applied Physics, Netherlands Institute for Metals Research and Zernike Institute for Advanced Materials, University of Groningen, Nijenborgh 4, 9747 AG Groningen, The Netherlands*

Received 28 October 2007; accepted 13 December 2007
Available online 7 February 2008

**Abstract**

Three glass-forming alloy compositions were chosen for ribbon production and subsequent electron microscopy studies. In situ tensile testing with transmission electron microscopy (TEM), followed by ex situ TEM and ex situ scanning electron microscopy (SEM), allowed the deformation processes in tensile fracture of metallic glasses to be analysed. In situ shear band propagation was found to be jump-like, with the jump sites correlating with the formation of secondary shear bands. The effect of structural relaxation by in situ heating is also discussed. Nanocrystallization near the fracture surface was observed; however, no crystallization was also reported in the same sample and the reasons for this are discussed. Both the TEM and the SEM observations confirmed the presence of a liquid-like layer on or near the fracture surface of the ribbons. The formation of a liquid-like layer was characterized by the vein geometries and vein densities on the fracture surfaces and its dependence on shear displacement, $\delta$, is discussed. A simple model is adapted to relate the temperature rise during shear banding to the glass transition and melting temperatures and this is used to explain the variety of fracture surfaces which are developed for macroscopically identical tensile testing of metallic glasses together with features which exhibit local melting.


*Keywords:* Metallic glasses; Electron microscopy; Shear bands; In situ; Tensile testing

## 1. Introduction

It is well understood that shear bands form in bulk metallic glasses (BMGs) as a plastic response to deformation at low temperatures [1,2]. Significant progress has been made in recent years in the understanding of the associated deformation and fracture in amorphous metals, together with possible control of shear band propagation by virtue of nanocrystalline additions in order to suppress the tendency for instantaneous catastrophic failure [3–7]. However, it is also apparent that there is still much inconsistency, and whilst many sound hypotheses and proofs abound, clarity is often lacking when comparing published results. Zhang et al. [8] review the high-resolution (HR) transmission electron microscopy (TEM) analysis of shear band thickness and find the range to be 10–20 nm for several BMG compositions. TEM should be a suitable tool for this kind of analysis of shear band formation in metallic glasses, since their thicknesses are very low and shear bands may be expected to lead to nanoscale structural changes in amorphous materials. However, this methodology often requires post-experimental sample preparation, which can invalidate TEM observations [9,10].

Analysis of inhomogeneous deformation of metallic glasses in compression and their response thereto has been extensively studied [11,12], since it is believed that this is the easiest manner in which to avoid catastrophic instability [13]. This consequently means that tensile fracture in BMGs has received less attention, mainly due to the high instability associated with plane stress and plane strain investigations. Some interesting tensile investigations have been reported [14], and in situ TEM has been shown to be an excellent tool for observing the formation of nanocrystals and their effects (such as crack blunting) [5].

* Corresponding author.
*E-mail address:* j.t.m.de.hosson@rug.nl (J.Th.M. De Hosson).

1359-6454/$34.00 © 2007 Acta Materialia Inc. Published by Elsevier Ltd. All rights reserved.
doi:10.1016/j.actamat.2007.12.029

It has been widely believed that shear in metallic glasses can develop high local temperatures [15,16], leading to a range of fracture surface features in metallic glasses [17], which can be simple, flat and almost featureless shear planes; have characteristic vein patterns formed by the meniscus instability [18] initiated from the surface edges or homogeneously inside a deformed layer; or have wide and very elongated veins extending along the shear surface from the edge of the shear step of bulk samples [17]. Again, there remains uncertainty over the differences in fracture surfaces [4], although Zhang et al. attempt to compare differences in compressive and tensile fracture surfaces in [19]. Analysis of these features, however, suggests that the heat developed during deformation in metallic glasses means that much more material is involved in the formation of a so-called "liquid-like layer" (LLL) [8] than the accepted width of a shear band (10–20 nm) [8,9].

Direct proofs of those temperature rises have been published, with the analytical methods including high-speed cameras in compressive and impact testing [20,21]. Recently Lewandowski and Greer [22] found a very elegant fusible-coating method to confirm experimentally the local temperature increase in the vicinity of a shear band formed in amorphous material, using a thin tin coating on their surface which melts up to some distance from a developed shear band. In the model calculation, they consider a shear band to be a planar source of heat with density $H$ (J m$^{-2}$) at time $t = 0$. The temperature increase at a distance $x$ to the both sides of shear band located at $x = 0$ is given by:

$$\Delta T = \left(\frac{H}{2\rho C\sqrt{\pi\alpha}}\right)\frac{1}{\sqrt{t}}\exp\left(\frac{-x^2}{4\alpha t}\right), \quad (1)$$

where $\rho$ is the material density, $C$ is the specific heat of the material and $\alpha$ is the material thermal diffusivity. Their measurements approved this relatively simple model as well as producing an estimation of the amount of heat released $H$, calculated from the uniaxial yield stress $\sigma_y$ and the shear displacement $\delta$ [16,30]:

$$H = \beta\sigma_y\delta, \quad (2)$$

where $\beta$ is a constant of value <0.35 in the case of 45° shear. Further experimental study [16] confirmed this model, showing that a linear dependence between shear displacement and width of melted coating area exists for three different metallic glasses with $\beta = 0.30$.Given that heat is developed during shear in metallic glass, it may be safe to assume that crystallization may occur within that heat-affected area. Published data have shown both that it does [4] and that it does not occur [14]; to the best of our knowledge, no explanation is offered for these differing findings.

In the current work, we attempt to address the problems outlined above by adopting the model engaged for the tin-coating investigations [22] and applying it to the glass transition temperature of a given material. We also attempt to estimate the thickness of the LLL by complimentary TEM and scanning electron microscopy (SEM) observations. Due to the nature of in situ TEM testing, the samples must be very thin and therefore the results should not be automatically assumed valid for normal "bulk" samples, although the compositions chosen are from BMG compositions. We address discrepancies in experimental and model findings, and discuss the formation of a range of fracture surfaces developed under macroscopically identical conditions for several BMGs, namely $Cu_{47}Ti_{33}Zr_{11}Ni_6Sn_2Si_1$ [23]], $Zr_{50}Cu_{30}Ni_{10}Al_{10}$ [24] and $Zr_{52.5}Cu_{17.9}Ni_{14.6}Al_{10}Ti_5$ (VIT105) [25].

## 2. Experimental procedure

Alloys were prepared by weighing the component elements, such that an approximately 1 cm$^3$ "button" could be produced by arc melting. The materials were of at least 99.99% purity, and in sheet, plate, pellet or powder form prior to fabrication. The melting process was conducted in a Ti-gettered, high-purity argon atmosphere. To ensure chemical and microstructural homogeneity, the buttons were rotated and remelted 3–5 times within the furnace. The resultant buttons were then weighed and (given negligible weight loss) analysed by light microscopy and SEM using a Philips XL30 FEG equipped for electron-dispersive spectroscopy (EDS). Ribbons of 2–8 mm width, with thicknesses in the region 20–50 μm, were produced from the pre-alloyed buttons by reheating above their melting point by induction heating in an argon or helium atmosphere and injected with an overpressure of 500 mbar onto a rotating (1800 rpm) copper wheel (Ø = 50 cm). The resultant ribbons were then confirmed to be amorphous by X-ray diffraction (XRD) (Phillips PW1710) and investigated using HRTEM (FEG Jeol 2010) with in situ heating and straining, along with EDS. Two sample dimensions were chosen for the in situ straining measurements, as shown in Fig. 1. In the in situ set-up of the JEOL 2010, one end is "clamped" while the other is extended at a desired extension rate. In these experiments, that strain rate was varied, but most results are shown for 0.1 μm s$^{-1}$ (corresponding to $10^{-5}$ s$^{-1}$) extension rates as this permits a reasonable

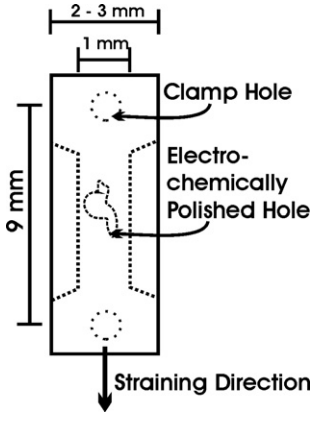


Fig. 1. Schematic representation of the sample dimensions used in in situ TEM straining.

propagation time without losing imaging capabilities. Larger strain rates will also be discussed.

## 3. Results

In order to investigate the effects of temperature, composition and strain rate on the development of shear bands in metallic glasses, the tensile stage in a high-resolution transmission electron microscope was chosen as the analytical tool. Prior to TEM investigation, all samples were confirmed X-ray amorphous using XRD technology and information regarding TEM heating parameters was attained using thermo (dynamic) testing. The results thereof will be revealed where necessary.

### *3.1. In situ TEM straining of $Cu_{47}Ti_{33}Zr_{11}Ni_6Sn_2Si_1$ BMG ribbon*

As an initial cautionary note, the in situ TEM straining observation of metallic glass ribbons was found to be a far from easy experiment since, in non-notched samples, the prediction of where a shear band may initiate is a matter of luck. However, a means has been found in situ by which the propagation of a shear band and its associated fracture tip may be followed and analysed. Fig. 2 relays a typical result for $Cu_{47}Ti_{33}Zr_{11}Ni_6Sn_2Si_1$ alloy. In Fig. 2A the state of the crack tip at 368 μm extension (=4.08% strain) is shown. The fracture opening is preceded by material thinning induced through the progression of the shear band. The shear band itself was initiated at around 3% strain, as may be expected for amorphous materials. After imaging at 368 μm extension, the sample was then re-strained for a further 3–371 μm extension (4.12% strain), accompanied with video recording. The time taken for this displacement to occur was 30 s (extension rate = 0.1 μm $s^{-1}$). No jerky motion was seen in this case, but instead the opening of the crack tip was seen to be constant; however, in some cases, applied load resulted in no discernible change at the crack tip for up to 5 μm normal extension. This is complementary to macroscale observations in shear band propagation. Imaging the new crack tip allows measurement of the crack tip displacement and crack tip characteristics (Fig. 2B). Little change in the microstructural appearance of the crack opening was seen. Characteristics of the area in and around the projected shear band include narrow (10–20 nm) featureless bands at the edge of the fracture surface. The next region is shown to be a speckled band, 20–50 nm in width. The features in the speckled region are 2–5 nm in size, but could not be resolved as crystals in HRTEM investigations. It may, therefore, be reasonable to consider the smooth, bright bands to be characteristic of the shear band, while in the speckled region, the nanoscale features can be attributed to very local meniscus instability.

An extension of 3 μm in the tensile loading direction ($\Delta l_n$) is found to translate to a crack propagation displacement ($\Delta l_p$) of 338 nm, heralding an approximate relationship of $\Delta l_n \approx 10\Delta l_p$ during plastic deformation. This relationship was confirmed over further observations, although instances whereby application of load led to no propagation in the direction of the shear band was also seen as stated above.

Upon further straining, the shear band propagates away from the electrochemically polished hole to the thicker "bulk" sample and this in turn leads to a change is stress state, which results in the formation of shear band branching since the character of the stress conditions at the surface (plane stress) are different to the conditions inside (plane strain) the sample, which means that not all shear

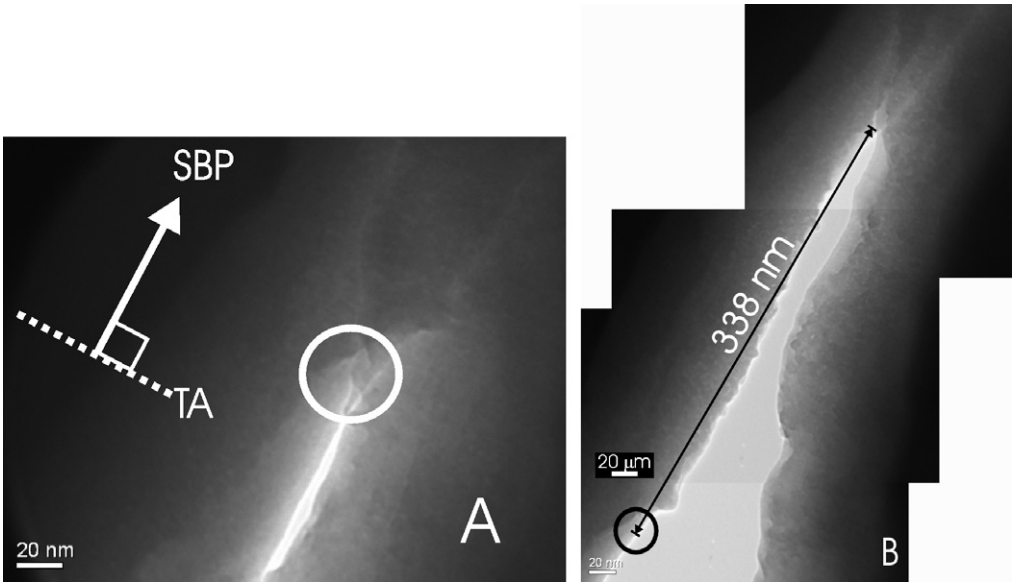


Fig. 2. (A) TEM micrograph of a shear band and its crack opening after 4.08% strain in $Cu_{47}Ti_{33}Zr_{11}Ni_6Sn_2Si_1$ alloy. The inset shows that the Shear Band Propagation (SBP) direction relative to the Tensile Axis (TA) was found to be (~) 90°. The white circle corresponds with the black circle in (B), a TEM micrograph of the crack opening progress at 4.12% strain.

bands which form lead to fracture, as seen in Fig. 3. The formation of secondary shear bands occurs when there is a temporary halt in the progression of the shear band due to competing planes of maximum shear stress. In the in situ observations here, the crack propagation along the primary shear band (in the plane of maximum shear stress) and the occurrence of the secondary shear band in the opposing plane were simultaneous.

In one special case, crystallization due to shear band formation was found. In this case, the propagation rate was much greater since, during the image collection, 25 full frames are recorded per second. Fig. 4B reveals the rapid crack propagation that occurred in one full frame with respect to Fig. 4A. Upon sighting this rapid propagation, the progressive loading was stopped immediately and the full extent of the crack movement was imaged. The length over which the crack existed was >600 nm.

At the head of this crack a meniscus was found, which signifies liquid-like behaviour, and all resolvable material ahead of this tip was shown by HRTEM to be amorphous (Fig. 5A). The edges of the sample close to the meniscus revealed crystallinity which must be developed due to the rapid segregation of the shear surfaces and the heat associated with that. Fig. 5B shows the crack tip developed in the $Cu_{47}Ti_{33}Zr_{11}Ni_6Sn_2Si_1$ ribbon shown in Fig. 2B. The difference is clear and the area around this crack tip remains amorphous. The results of this rapid propagation will be discussed later.

### 3.2. In situ TEM straining of $Zr_{50}Cu_{30}Ni_{10}Al_{10}$ BMG ribbon plus "post-mortem" SEM

The shear band initiation and crack propagation of this alloy was found to be similar to that outlined above; however, in some cases "full fracture" is induced rapidly; here we define full fracture as the fracture induced by deformation due to shear banding of the sample through its full thickness between any two free ends. Given the nature of the test, this does not mean that the sample is necessarily split in half, since electrochemical polishing often results in more than one hole. In all cases where this kind of fracture occurred, the initial shear band was not seen before full fracture occurred. The resultant sample surface was, however, found to be the same in all cases and was characterized by edge thinning, with short corrugated veins being observed at one end of the fractured plane, as seen in Fig. 6A. HRTEM raises questions over possible crystallization or atomic ordering during shear band propagation, as shown in Fig. 6B, which is a micrograph from the vein tip shown in Fig. 6A. Surprisingly, these veins were only seen at one end of the fractured section.

Post-mortem SEM (Fig. 7A and B) reveals that the end at which the veins appeared was the end of final contact. The two fracture surfaces overlap one another in these figures because of sample retraction when the load was removed from the tensile stage. It is not believed that this added any extra deformation to the sample.

The fact that the ribbon is less than 2 μm in thickness may play in a role in the development of an LLL since no veins appear on the fracture surface itself. This will be discussed later. Several other interesting features can be seen in this analysis. The shear band propagates in tearing mode from left to right in the images of Fig. 7 in a direction approximately perpendicular to the tensile stress component, while the shear band planes are inclined to the ribbon surface plane. The shear band initially appears to propagate as a straight line. As the sample thickness increases, a few secondary shear bands appear, all in roughly parallel planes. The shear crack propagated with a jump-like motion. A jump site may be detected via a characteristic set of secondary shear bands at the place when failure stopped momentarily to select a new plane for further propagation. As seen for $Cu_{47}Ti_{33}Zr_{11}Ni_6Sn_2Si_1$ alloy (Fig. 3), the branches are developed at these jump sites and the point at which the shear offset is developed occurs very rapidly indeed.

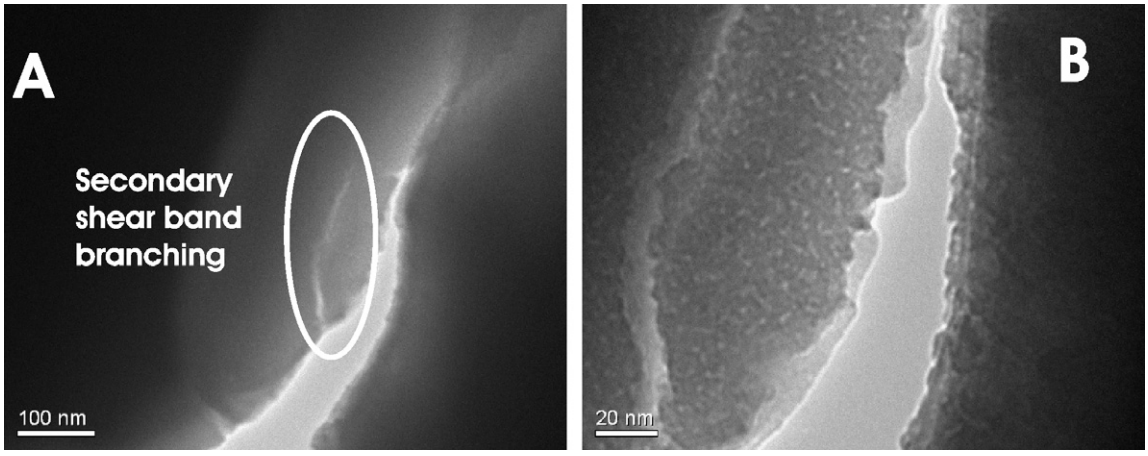


Fig. 3. (A) and (B) TEM micrographs revealing shear band branching in $Cu_{47}Ti_{33}Zr_{11}Ni_6Sn_2Si_1$ ribbon at 4.4% strain. The white ellipse in (A) highlights the secondary shear band, while the white ellipse in (B) highlights an area of speckled appearance.

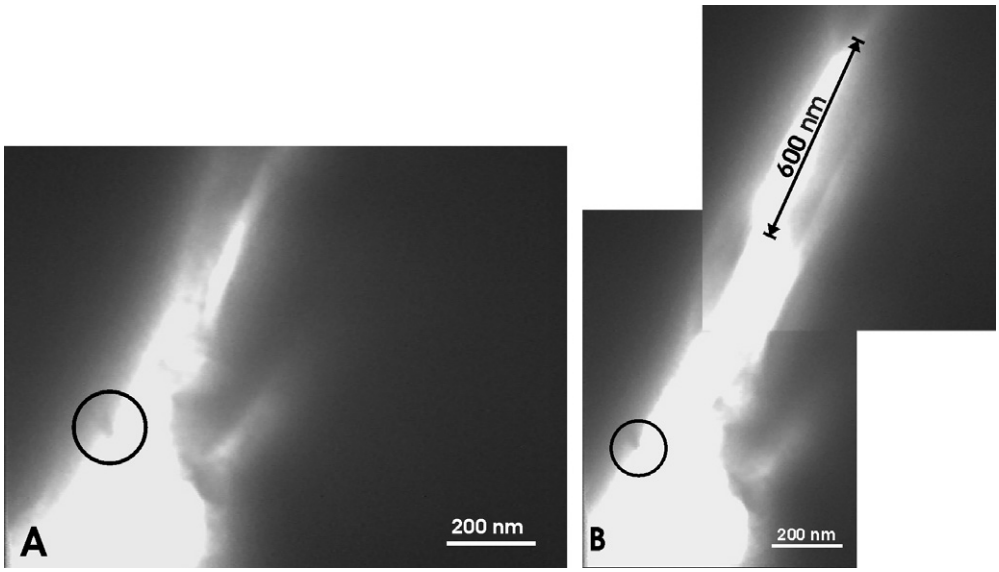


Fig. 4. Rapid fracture in $Cu_{47}Ti_{33}Zr_{11}Ni_6Sn_2Si_1$ ribbon. The black rings highlight corresponding areas in (A) and (B).

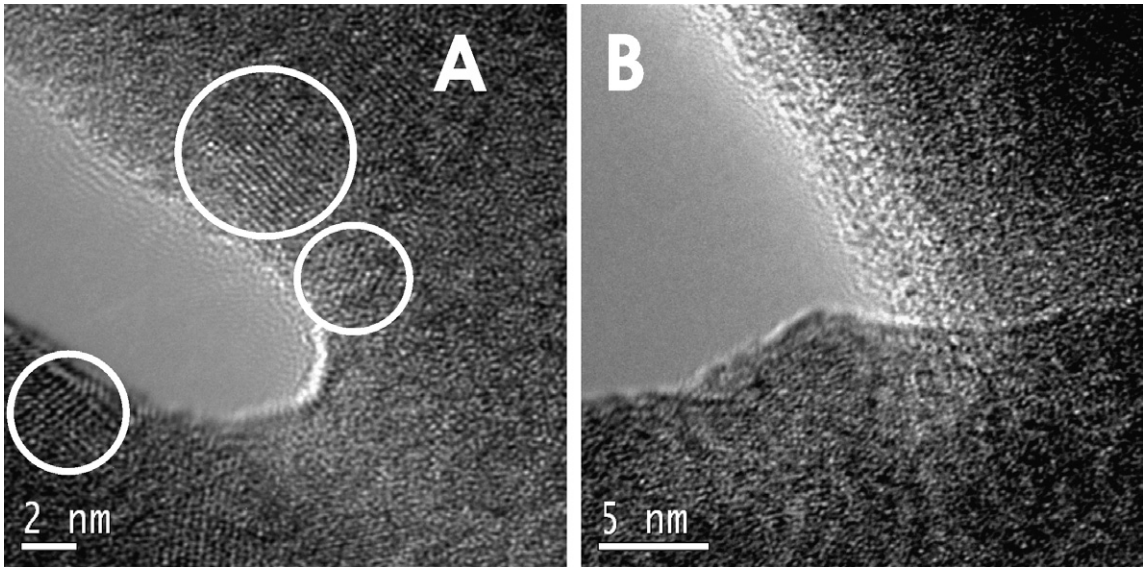


Fig. 5. HRTEM micrographs revealing (A) a rapid-propagation induced meniscus at the crack tip and (B) no meniscus in 'controlled' propagation shown in Fig. 2b for $Cu_{47}Ti_{33}Zr_{11}Ni_6Sn_2Si_1$ ribbon.

### *3.3. In situ TEM straining of $Zr_{52.5}Cu_{17.9}Ni_{14.6}Al_{10}Ti_5$ (VIT105) BMG ribbon and the effect of in situ heating plus "post-mortem" SEM*

Glass-forming alloy VIT105 ($Zr_{52.5}Cu_{17.9}Ni_{14.6}Al_{10}Ti_5$) has been the subject of many recent investigations. Here we examine it by in situ tensile testing as described earlier, but with three changes to the procedure. First, the samples are also prepared with a dogbone-like geometry (Fig. 1); secondly, the extension rate is higher (1 μm $s^{-1}$ = strain rate $\sim 10^{-4}$ $s^{-1}$); and thirdly, elevated temperature (with respect to room temperature) experiments were conducted. The aim of the raised temperature investigation was to bring the alloy as close to $T_g$ as possible without inducing crystallization; however, one of the drawbacks of in situ TEM heating is control of the sample temperature. In these results, the sample chamber was elevated to above 773 K ($T_x$ for this alloy has been found to be 714 K), but no crystallization was seen. Therefore the actual sample temperature must still have been below $T_x$. Although the exact sample temperature is unknown, it can be safely assumed that the alloy underwent (limited) structural relaxation.

Results from the sample subjected to room temperature deformation show the sample to fail in full fracture in an area away from the electrochemically polished region. Results from both simple shear-band-initiated samples and full-fracture samples were recorded.

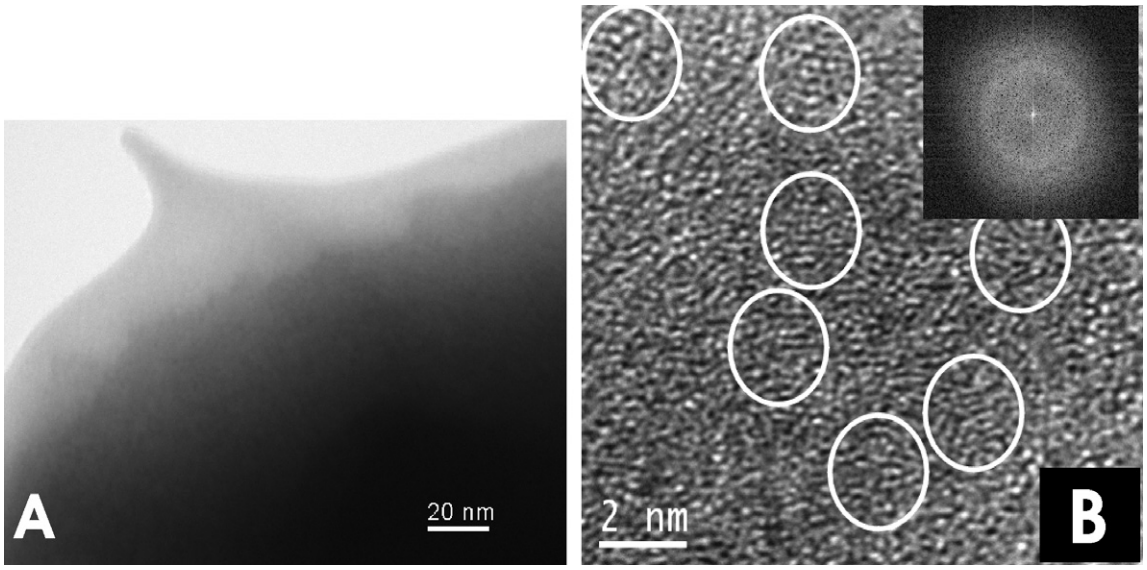


Fig. 6. (A) TEM micrograph revealing a ~20 nm triple point vein tip and (B) a high-resolution TEM image of the vein tip revealing possible nanometer scale ordering, but this in unconfirmed in the FFT inset for $Zr_{50}Cu_{30}Ni_{10}Al_{10}$ ribbon.

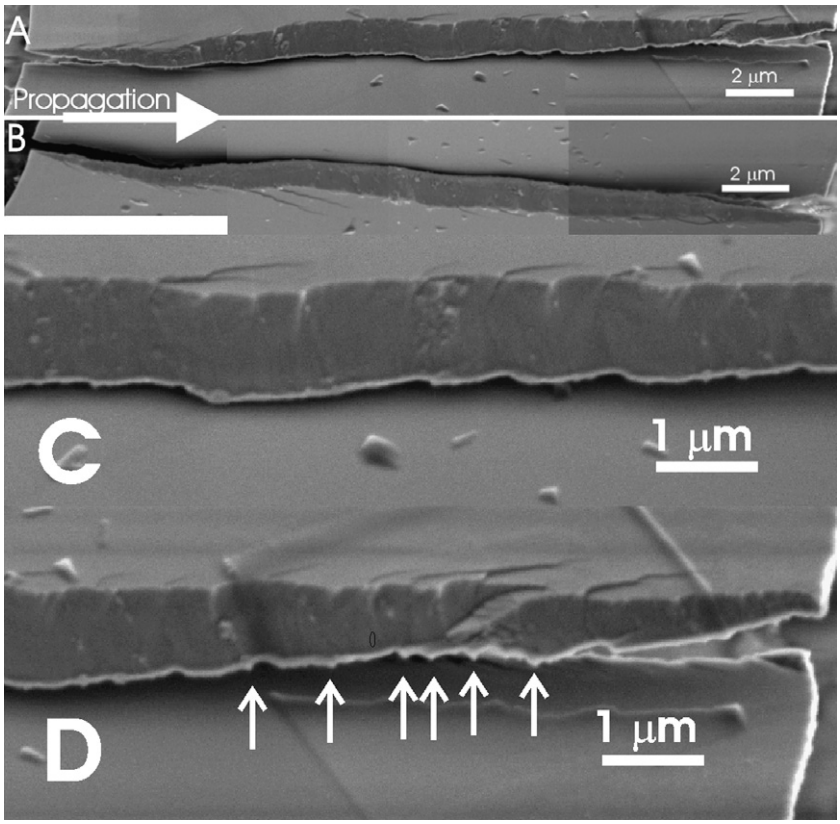


Fig. 7. SEM micrographs revealing the corresponding fracture surfaces of (A) "top" and (B) (mirrored) "bottom" sections of a section of $Zr_{50}Cu_{30}Ni_{10}Al_{10}$ ribbon which underwent 'full fracture' driven by shear band propagation (C) fracture surface revealing no liquid-like behaviour and (D) fracture surface at propagation end revealing material shear, but no liquid-like behaviour, except at the final points of contact which are highlighted by the white arrows.

In the example shown here, full fracture did not occur. The shear band detected by HRTEM (Fig. 8A) shows the typical crack opening behaviour seen already with other amorphous alloys and remained amorphous (HRTEM 8A), while post-straining SEM analysis showed the presence of many secondary shear bands. The fracture surface (Fig. 8B), however, did not reveal any liquid-like behaviour. The material involved in the shear process did not

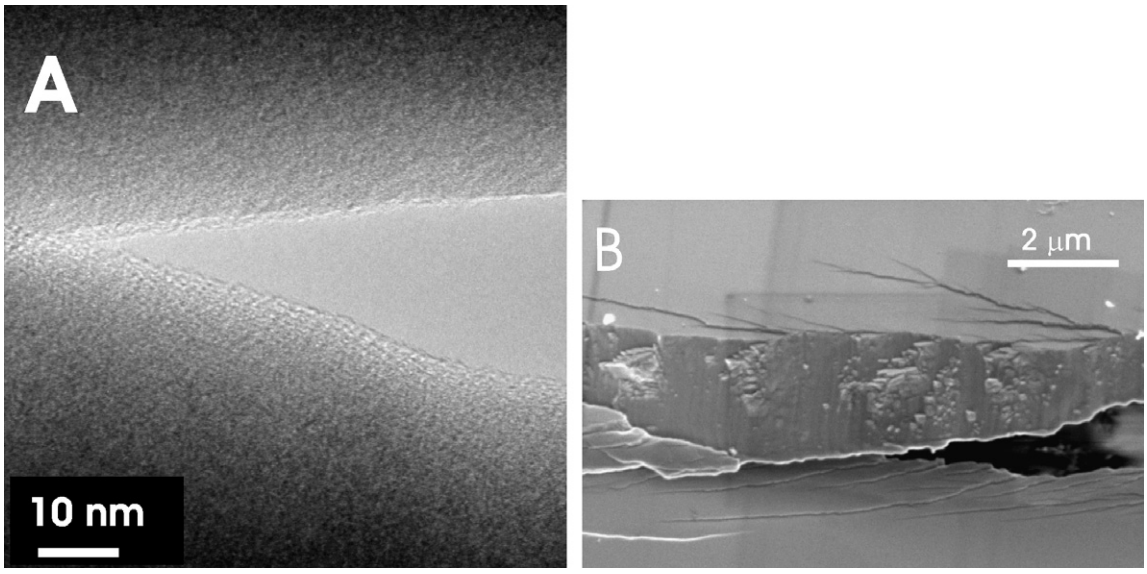


Fig. 8. (A) HRTEM image showing the crack opening; (B) is an SEM micrograph revealing no evidence of surface feature heating/melting despite full surface separation for $Zr_{52.5}Cu_{17.9}Ni_{14.6}Al_{10}Ti_5$ ribbon.

have an appearance which would suggest it had experienced significant heating, but it had clearly been sheared across the fracture surface and remained intact with the surface. The individual features on the fracture surface range in size from a few hundred nanometers up to 1 μm. It is interesting to note that the shear displacement $\delta$ which develops in the secondary shear bands (e.g. Fig. 8B) does not travel past the centre of the ribbon, and secondly, that in the images where this occurs, the effect is not mirrored on the ribbon's underside. This may suggest that a certain degree of the (secondary) shear band deformation may be absorbed plastically.

The formation of veins in the full-fracture sample was again seen because of meniscus instability and their lengths were spread over a wider scale, the veins being much longer than those seen in the previous case (see section 3.2). This suggests that more material is involved in the formation of an LLL during deformation. Fig. 9A shows one of these triple-point veins. Their lengths range from 200 to 600 nm, and they could be found across the whole length of the fracture surface. Fig. 9B confirms these vein nipples to be amorphous for a sample heated to 703 K in a TEM chamber.

If the unheated sample is viewed in "post-mortem" SEM, the result shows typical fracture surfaces associated with failure in metallic glasses. Fig. 10A shows such a surface. The veins witnessed by TEM are again visible during SEM analysis and their average height and density may therefore be calculated, as will be discussed below in Section 4. While the shear angle was seen to be consistent around 53°, the primary shear plane on which it propagated was seen to alternate (Fig. 10B).

When the sample chamber is heated to 430 °C, the veins which develop are found to be characteristically different. Fig. 11A shows a series of short veins developed during tensile fracture at elevated temperature, while some veins are clearly faceted at the root and are much longer (up to 2 μm) (Fig. 11B). HRTEM again, however, revealed no crystallization.

The fracture surface again revealed many triple-point veins up to 2 μm in length, as seen by the TEM. There was also evidence of shorter veins and material melting, since the surface artefacts form liquid-like balls (spheroid drops), as shown in Fig. 12A, compared with the surface debris artefacts in Fig. 8B, which do not exhibit liquid-like features. The fracture angle in a given plane was found to be 53° (Fig. 12B), which is in excellent agreement with previous research on the fracture angle of metallic glasses in tension.

## 4. Discussion

### 4.1. Experimental analysis of the LLL thickness

The term "liquid-like layer" is currently used quite frequently in the literature in connection with catastrophic shear fracture of metallic glasses. However, more than 30 years ago, Takayama and Maddin [26] suggested a "grease" model, which gave a good simulation of the actual fracture morphology of metallic glass ribbon. Recently, Zhang and Greer concluded in their review [8] that the shear localization in metallic glasses is the cause of the temperature rise and not its consequence. Therefore, the shear band formation is only the first stage of catastrophic failure and it takes a time of the order of a nanosecond [22]. In the following stages of the catastrophic shear failure, a subsequent temperature increase due to the thermal diffusion from the shear band to the surrounding volume and a redistribution of local stresses due to the shear deformation take place. The vein pattern morphology on the fracture surface is

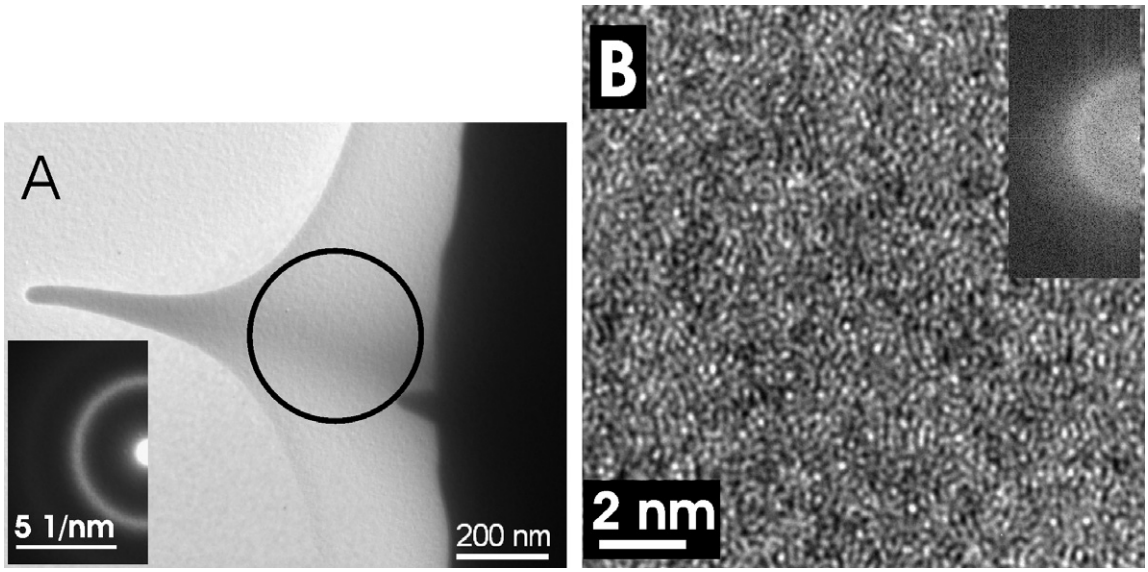


Fig. 9. (A) TEM micrograph revealing a triple point vein formed in $Zr_{52.5}Cu_{17.9}Ni_{14.6}Al_{10}Ti_5$ alloy. The inserted SAED ring is taken in the area highlighted by the black circle and shows the vein to be fully amorphous. (B) This was confirmed at the vein tip by HRTEM and FFT.

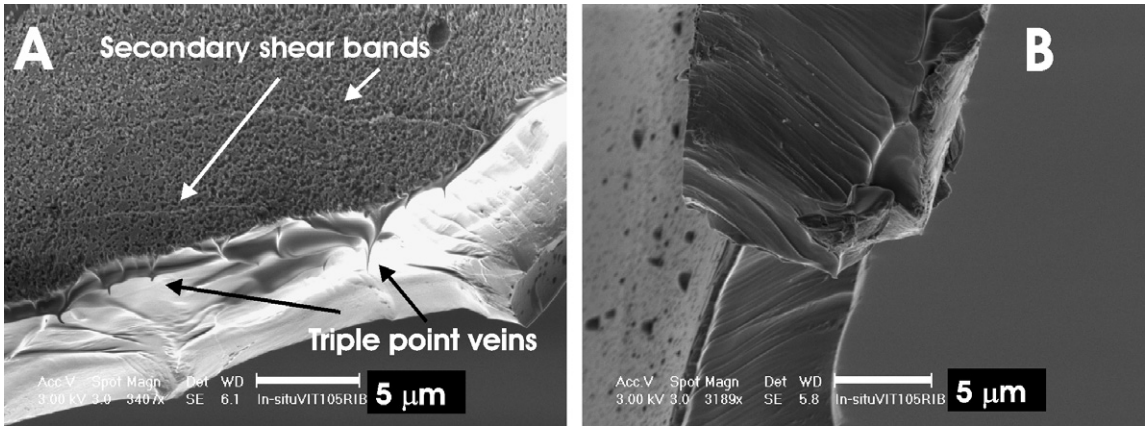


Fig. 10. SEM micrographs revealing (A) the formations of triple point veins and secondary shear bands and (B) alternating shear planes in VIT105 glassy ribbon as indicated by the white arrows.

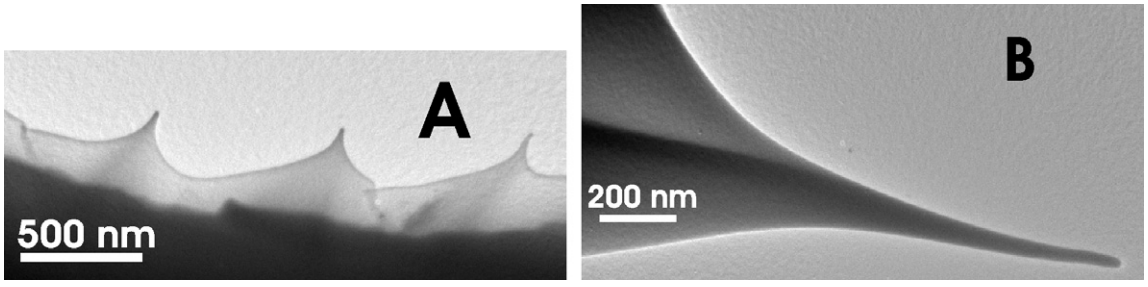


Fig. 11. (A) A series of veins exhibiting their inter-vein spacing and (B) a very elongated vein produced during failure of VIT105 ribbon elongated in a TEM chamber at 430 °C.

formed during the very last stages of the fracture when there are appropriate conditions for meniscus instability to occur. These conditions include appropriate thickness, viscosity and surface tension of the LLL, as well as the presence of a normal stress component [18].

We used the combination of TEM and SEM observations of features on the fracture surfaces exhibiting vein patterns to estimate the lowest limit of the amount of material that is active during the last moments of failure. Quantitative analysis of a group of TEM observations of veins

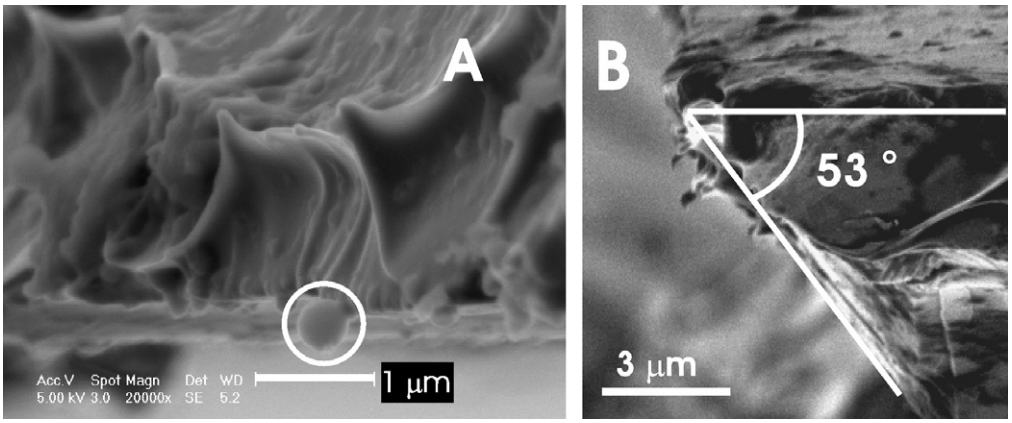


Fig. 12. SEM micrographs revealing: (A) short triple-point vein tips (>1 μm) and apparent melting with the presence of spheroid drops ~300–500 nm in diameter adhered to the fracture surface and (B) the fracture angle for $Zr_{52.5}Cu_{17.9}Ni_{14.6}Al_{10}Ti_5$ alloy pulled in tension to failure at 10–4 $s^{-1}$ side-on vein tips can bee seen on the fracture surface.

similar to Fig. 9A allows us to estimate the average height of a vein as 0.31 μm, and to approximate its profile as an isosceles triangle with the same base in accordance with scanning tunnelling microscope observations [27]. A linear density of veins on the fracture surface may be directly estimated using one of the statistical methods of quantitative stereology [28] applied to SEM micrographs, similar to Fig. 14, where the fracture surface of VIT105 ribbon exhibits a characteristic vein pattern area.

Simply counting the number of intersections of veins with randomly applied grid lines inside the vein pattern area, calculating the average number of these intersections per unit length and multiplying by a constant $\pi/2$ gives us the average linear density of veins on a fracture surface of VIT105 alloy $= 1.25\ \mu m\ \mu m^{-2}$. Multiplying this average linear vein density by the average vein profile estimated from TEM observations, we get the volume of 0.061 $\mu m^3$ per each $\mu m^2$ of fracture surface. Assuming that the major part of the LLL during failure is moving into the veins and that the vein pattern is mirrored at the opposite side of fractured surface [26], we estimated the lowest limit of thickness of LLL to be 120 nm.

There is another approach to estimating the thickness of the LLL [8], based on the fact that the meniscus instability process starts at air in an LLL of a thickness about 2–20 times the vein spacing at the site of initialization [18]. Measuring the value of average vein spacing at the places similar to the area around the initiation core shown in Fig. 15A, we obtained a value of 0.27 μm, which results in an estimation of thickness of the LLL of between 0.5 and 5 μm.

Both these estimations substantially exceed the thickness of a single shear band, which verifies our expectation that much more material is taking part in the last stage of the failure process than the volume of a single shear band.

### 4.2. Theoretical heat release and LLL thickness

The fact that veins are seen to develop on some fracture surfaces but not on others, and the fact that the appearance of the fracture surfaces can be so very varied, means that the local temperature and/or active stress components must be different in the various cases. There is clear evidence of elevated temperatures, since the (last point of contact) failure becomes ductile in appearance due to necking. The question, of course, is how high is this local temperature? In order for ductile fracture to occur in metallic glasses, viscoplastic deformation must be induced. One manner in which viscoplastic deformation is induced [29] is when the material temperature is raised. The temperature regime in which the material behaves viscoplastically can be determined through thermomechanical analyses. The behaviour is associated with the glass transition temperature, which has been shown to be 672 K for VIT105 alloy. The temperature at which the crystallization starts, $T_x$, is 714 K; however, high heating rates can substantially increase this value.

Bengus at al. [30] hypothesized as early as 1993 that extreme local heating and melting may occur at the shear crack front developed during tensile tests of amorphous alloy ribbons. Their deductions were supported by the measurement of kinetics of shear crack propagation, by the estimation of the amount of elastic energy released and transformed to the local heat in an extremely short time and by the observations of spheroid drops on the fracture surface of $Fe_{83}B_{17}$ amorphous alloy ribbon. Fractographic evidence of the local hot state of the material on the shear failure surfaces was also found for amorphous ribbons tested in tension at very low temperatures (4.2 K) [31] and for bulk amorphous alloys tested in compression [17].

Fracture surfaces of amorphous ribbons or bulk amorphous materials studied during recent decades have shown a variety of fractographic features, from simple, flat and almost featureless shear planes (as in Fig. 7 and left upper part of fracture surface in Fig. 14), via characteristic vein patterns formed by the meniscus instability [18] initiated from the surface edges (bottom part of Fig. 14) or homogeneously inside a deformed layer (Fig. 15A), to wide and

very elongated veins extending along the shear surface from the edge of the shear step of bulk samples [17]. However, from all these observations it seems that much more material is involved up to the final fracture process than corresponds to the generally accepted width of the shear band, ~20 nm [9], confirmed recently also by MD calculations [32]. Moreover, some TEM observations confirmed the presence of crystalline nuclei of different sizes near the shear crack tip or fracture surface [4,5,9].

According to the contemporary concept of shear band formation in amorphous metals [8,16,22], immediately after instantaneous shear band development, the surrounding amorphous material is heated up from the environment temperature $T_0$ due to heat diffusion. The volume where the local temperature is higher than the glass transition temperature $T_g$ may be deformed easily due to substantially decreased viscosity, when both tensile and shear stress components exist.

The size of this volume for alloy VIT105 may be estimated using Eq. (1). We assumed $\sigma_y = 1850$ MPa, $\rho = 6600$ kg m$^{-3}$ [33], $C = 420$ J kg$^{-1}$ K$^{-1}$, $\alpha = 3 \times 10^{-6}$ m$^2$ s$^{-1}$ and $T_g = 674$ K [34]. Fig. 13 relays our calculations. Fig. 13A shows one-half of the temperature increase profile in the vicinity of a single shear band with a shear displacement, $\delta = 5$ μm (a value near to that observed in Fig. 14), at three different times, 3, 12 and 50 ns, respectively. The horizontal line made at $\Delta T = 376$ K corresponds to the limit when the temperature increase from room temperature reaches the glass transition temperature $T_g$. From Fig. 13A it can be concluded that the volume which may be considered to be at a temperature over $T_g$ is dependent on time. At a time shortly after shear band development (3 ns), the temperature increase is relatively high; however, the heat-affected volume is small. After 50 ns, all material is cooled down under $T_g$. If one would like to know the maximal distance to which the material is overheated over the glass transition temperature, the differentiation of Eq. (1) gives the value of maximum temperature increase together with the time at which this maximum is reached. This calculation is shown in Fig. 13B for four different shear displacements: 1, 5, 10 and 50 μm. It is seen that 5 μm shear displacement may induce, at time 17 ns, a viscoplastic layer with a thickness slightly exceeding 0.6 μm. A 1 μm shear displacement offers only a 0.13 μm layer for a much shorter time and the larger displacements, such as 10 and 50 μm, usually observed on the fracture surfaces of bulk amorphous samples, may form much thicker, liquid-like layers (1.3 and 6.4 μm) for substantially longer times (70 ns and 1.7 μs).

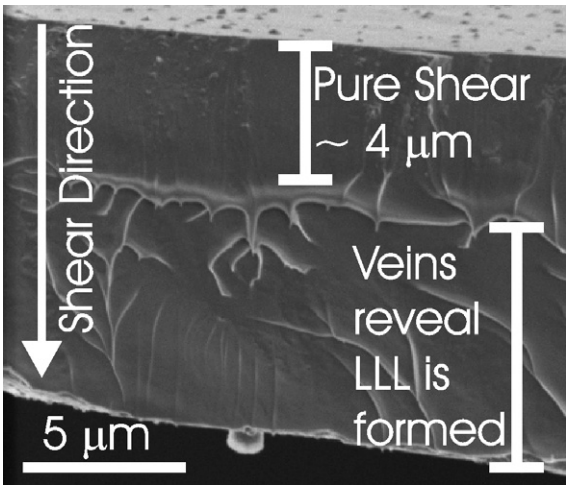


Fig. 14. SEM micrograph revealing a fracture surface of VIT105 ribbon strained at room temperature to failure at $1 \times 10^{-4}$ s$^{-1}$. LLL = liquid-like layer.

The horizontal line $\Delta T = 740$ K that corresponds to the temperature increase over the melting temperature of VIT105 glass [34] is also presented in Fig. 13A and B to indicate that a large displacement offers enough heat for local melting, as the spheroid drop on Fig. 12A testifies.

Using Eqs. (1) and (2), we may calculate the half width $x_{T_g}$ of the zone around the shear band, within which the glass transition temperature would be exceeded, and the time when it happens. $x_{T_g}$ scales with $\delta$:

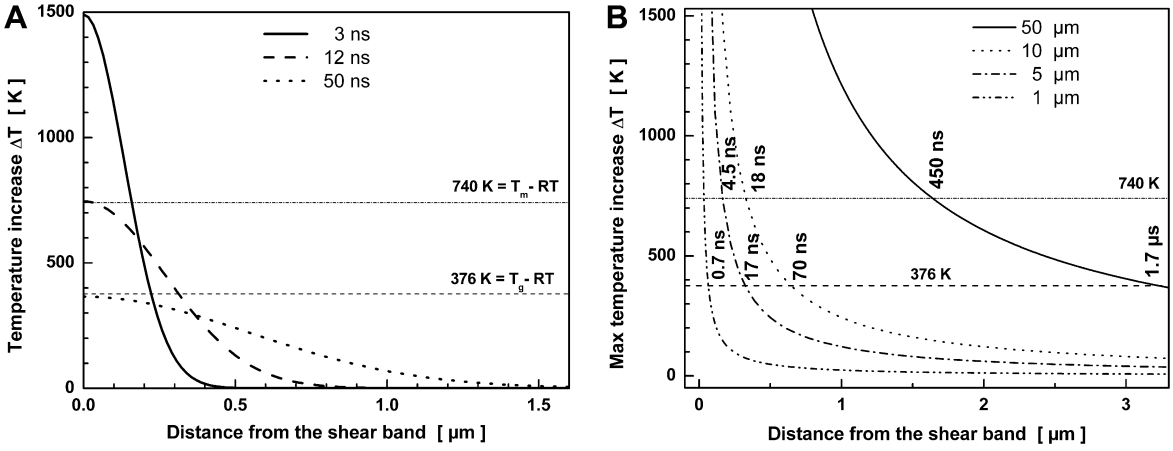


Fig. 13. (A) Local temperature increase in shear band vicinity calculated for a shear displacement, $\delta$, of 5 μm ($H = 1.34$ kJ/m$^2$) and $t = 3$, 12 and 50 ns for VIT105 alloy. (B) Maximum temperature increase calculated for shear displacements, $\delta = 1$, 5, 10 and 50 μm.

$$x_{T_g} = \frac{\beta}{\sqrt{2\pi e}} \frac{\sigma_y \delta}{\rho C (T_g - T_0)}. \quad (3)$$

The time when $T_g$ at distance $x_{T_g}$ is reached scales with $\delta^2$:

$$t_{T_g} = \frac{1}{4\pi e \alpha} \left( \frac{\beta \sigma_y \delta}{\rho C} \right)^2 \frac{1}{(T_g - T_0)^2}. \quad (4)$$

When we calculate the maximal thickness of LLL using the model approach explained above, we get for 3.5 μm shear displacement in this alloy a thickness of about 450 nm in 8.5 ns. This number is almost four times greater than our experimental estimation calculated from vein profile and density. However, two corrections to the experimental observations and model assumptions can account for this discrepancy. Firstly, the assumption that all liquid-like material is transformed into the veins is not realistic; a substantial fraction of the liquid-like material must remain indistinguishable by SEM on the fracture surface as a thin uniform layer. This assumption moves the estimated value of 120 nm for thickness of LLL to a higher value. Secondly, the final fracture will not wait until a maximum thickness of LLL is developed, but instead it can begin earlier, when a suitable thickness for meniscus instability formation is achieved. This fact corrects the calculated value 450 nm towards a lower value. To conclude, these two corrections bring the experimental value (which can be regarded as a lower limit) and the model value (which can be regarded as an upper limit) towards a more realistic value of the true volume of liquid-like material generated during shear band deformation.

Since it is clear that the shear displacement is the important influencing factor as regards LLL thickness, it is also reasonable to suggest that limiting the shear offset will limit the probability of inducing meniscus instability. Experimental observations reveal that pure shear presides up to 4 μm (Fig. 14) and samples thinner than this value exhibit no vein morphology, despite full fracture (Figs. 7 and 8). Therefore, in order to avoid catastrophic fracture by meniscus instability, for room temperature tensile deformation of metallic glass ribbons, restraining shear bands displacement to $\delta < 4$ μm may be a solution.

If the ambient temperature is brought close to $T_g$ during in situ TEM straining, a substantial increase in the plasticity and the amount of material involved in the veins formed was detected (see Figs. 11B and 15A). Inserting $(T_g - T_0) = 50$ into Eqs. (3) and (4), we obtain an LLL thickness of around 5 μm for 5 μm displacement in time 1 μs. These values are much larger than the values calculated and observed for room temperature experiments.

A variety of the fractographic features observed on the fracture surfaces of amorphous ribbons and bulk metallic glasses as well as possible crystallization events that occur near the shear band have been shown and discussed. The reasons for these variations are explained by the large number of parameters that influence the thickness of the LLL (scaling linearly with shear displacement) and the lifetime of an LLL (scaling with the square of shear displacement) in the vicinity of a shear band at the moment of failure. From the above analysis, we conclude that the thickness of the LLL depends, besides the shear displacement, upon the yield stress, the glass transition temperature, the ambient temperature and the local structural inhomogeneities that may initiate meniscus instability.

### 4.3. Nanocrystallization

A question remains as to why the local crystallization near a shear band is confirmed in some TEM observations [35] but not in others [14]. In our observations we also found small crystals (<5 nm in diameter) in the close vicinity (~10 nm) of a shear band observed in alloy $Zr_{50}Cu_{30}$-

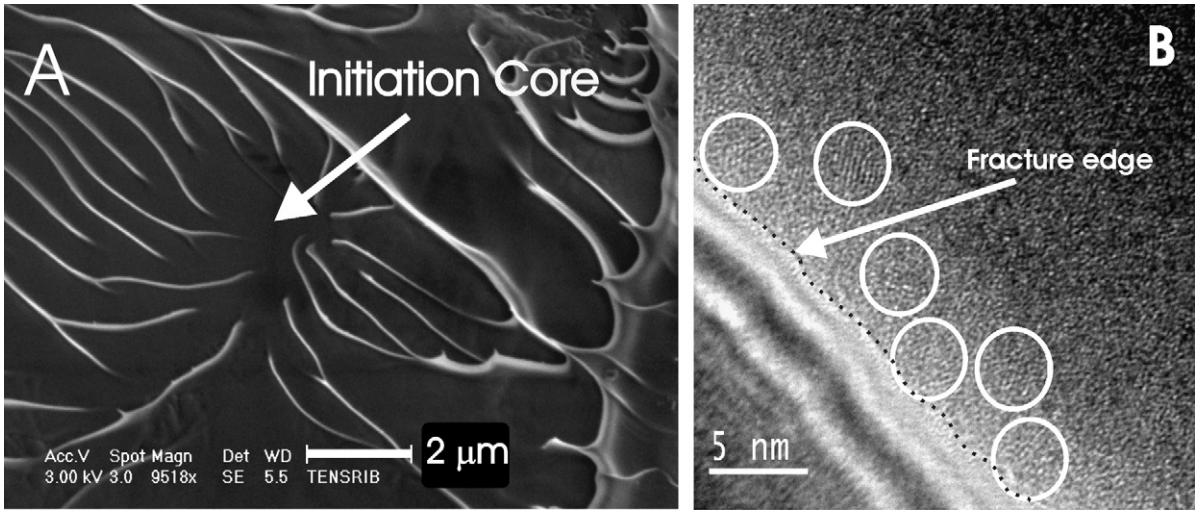


Fig. 15. (A) SEM micrograph showing the initiation place for meniscus instability in heated (430 °C) VIT105 and (B) HRTEM image revealing nanocrystallization close to the fracture surface edge for $Zr_{50}Cu_{30}Ni_{10}Al_{10}$.

$Ni_{10}Al_{10}$ in one case when it underwent "full fracture" (as shown in Fig. 15B). Crystallization was also seen in Section 3.1 when the alloy $Cu_{47}Ti_{33}Zr_{11}Ni_6Sn_2Si_1$ was shown to exhibit rapid crack propagation. Again, the crystallized zone comprised crystals <5 nm in size over a width of approximately 10 nm. Conversely, the HRTEM imaging of vein tips did not confirm that any crystalline phase was present. In the examples outlined in this work, where crystallization processes are derived, they are driven by temperature increases and not by deformation processes as reported elsewhere [4,35]. The most important influencing factor in this case is not the maximum temperature, but the time during which the heated volume stays at an elevated temperature, which must, due to the extreme heating rates, be much higher than conventionally measured $T_x$ (~500 °C). As has been shown in Fig. 13 and Eq. (4), this time scales with the square of shear displacement, $\delta$. However, for large shear displacements (~50 μm), the time at which the material is elevated above the measured $T_x$ is still less than 1 μs, which may be adequate for crystal growth but is insufficient for crystal nucleation, since the activation energy for nucleation is larger than the activation energy for crystal growth in amorphous alloys [36]. This explains why crystals only appear in a very narrow band at the shear band edge and also why those crystals are of nanometer size. Elsewhere [4], crystal growth up to almost 50 nm has been reported. This study supports that observation since the alloys (often Al based) have poor glass-forming ability and often contain nucleation sites already of nanometer size. The formation of larger crystals is therefore easier to facilitate.

## 5. Conclusions

Shear band propagation has been found to be jump-like by in situ straining in TEM. The secondary shear bands form a branch when the primary shear band stops and one of them will become the new primary shear band with the largest shear displacement, $\delta$.

Both TEM and SEM observations confirm the presence of an LLL on or near the fracture surface of the amorphous ribbons.

Estimations based on quantitative fractographic observations and model calculations permit an evaluation of the thickness of the LLL formed due to heat evolution after shear band development. Both experimental evaluation and model calculation confirmed that the thickness of an LLL present at the last moment of fracture substantially exceeds the generally accepted thickness of a shear band.

The probability of witnessing a crystal phase near the fracture surface is mainly dependent on the size of the shear displacement.

Limiting amorphous "features" within a material to <4 μm is recommended in order to avoid catastrophic fracture via meniscus instability.

## Acknowledgements

The authors gratefully acknowledge the financial support of Stichting FOM (Utrecht) and The Netherlands Institute of Metals Research. The authors are grateful to Prof. VZ. Bengus for his critical reading of the manuscript. Our warmest gratitude is also extended to Dr. P. Švec and D. Janičkovič at the Institute of Physics, Academy of Sciences (Bratislava), for the preparation of the ribbons.

## References

[1] Argon A. Acta Metall 1978;27:47–58.
[2] Spaepen F. Acta Metall 1977;25:407–15.
[3] Eckert J, Das J, Pauly S, Duhamel C. J Mater Res 2007;22:285–301.
[4] Gao MC, Hackenberg RE, Shiflet G. Mater Trans 2001;42:1741–7.
[5] Hajlaoui K, Yavari AR, Doisneau B, LeMoulec A, Botta WJ, Vaughan G, et al. Scripta Mater 2006;54:1829–34.
[6] Hajlaoui K, Doisneau B, Yavari AR, Botta WJ, Zhang W, Vaughan G, et al. Mater Sci Eng A 2007;449–451:105–10.
[7] Hufnagel TC, Fan C, Ott RT, Li J, Brennan S. Intermetallics 2002;10:1163–6.
[8] Zhang Y, Greer AL. Appl Phys Lett 2006;89:071907.
[9] Donovan PE, Stobbs WM. Acta Metall 1981;29:1419–36.
[10] Jiang WH, Atzmon M. Acta Mater 2003;51:4095–105.
[11] Lee JY, Han KH, Park JM, Chattopadhyay K, Kim WT, Kim DH. Acta Mater 2006;54.
[12] Lu J, Ravichandran G, Johnson WL. Acta Mater 2003;51:3429–43.
[13] Sergueeva AV, Mara NA, Kuntz JD, Branagan DJ, Mukherjee AK. Mater Sci Eng A 2004;383:219–23.
[14] Rizzi P, Battezzati L. J Non-Cryst Solids 2004;344:94–100.
[15] Spaepen F. Nat Mater 2006;5:7–8.
[16] Zhang Y, Stelmashenko NA, Barber ZH, Wang WH, Lewandowski JJ, Greer AL. J Mater Res 2007;22:419–27.
[17] Bengus VZ, Tabachnikova ED, Miskuf J, Csach K, Ocelik V, Johnson WL, et al. J Mater Sci 2000;35:4449–57.
[18] Argon A, Salama M. Mater Sci Eng 1976;23:219–30.
[19] Zhang ZF, Eckert J, Schultz L. Acta Mater 2003;51:1167–79.
[20] Jiang WH, Fan GJ, Liu FX, Wang GY, Choo H, Liaw PK. In: Liaw PK, Buchanan RA, editors. Bulk Metallic Glasses. Warrendale, PA: TMS; 2006.
[21] Yang B, Morrison ML, Liaw PK, Buchanan RA, Wang G, Liu CT, et al. Appl Phys Lett 2005;86:141904–07.
[22] Lewandowski JJ, Greer AL. Nat Mater 2006;5:15–8.
[23] Park ES, Lim HK, Kim WT, Kim DH. J Non-Cryst Solids 2002;298:15–22.
[24] Inoue A, Zhang T, Masumoto T. Mater Trans JIM 1990;31:177.
[25] Lin XH, Johnson WL, Rhim WK. Mater Trans JIM 1997;38:473.
[26] Takayama S, Maddin R. Philos Mag 1975;32:457.
[27] Kulawansa DM, Dickinson JT, Langford SC, Watanabe Y. J Mater Res 1993;8:2543–53.
[28] Russ JC, Dehoff RT. Practical stereology. 2nd ed. Dordrecht: Kluwer Academic/Plenum Publishers; 2000.
[29] Argon AS, Shi LT. Acta Metall 1983;31:499–507.
[30] Bengus V, Tabachnikova ED, Shumilin SE, Golovin YI, Makarov MV, Shibkov AA, et al. Int J Rapid Solidif 1993;8:21–31.
[31] Bengus V, Tabachnikova E, Csach K, Miskuf J, Ocelik V. Scripta Mater 1996;35:781–4.
[32] Shi Y, Falk ML. Phys Rev Lett 2005;95:095502–06.
[33] Wang WH, Dong C, Shek CH. Mater Sci Eng R 2004;44:45–89.
[34] Xing D, Sun J, Shen J, Wang G, Yan M. J Alloys Compd 2004;375:239–42.
[35] Jiang WH, Pinkerton FE, Atzmon M. Scripta Mater 2003;48:1195–200.
[36] Lu K, Wang JT. Mater Sci Eng A 1991;133:500–3.